The vibrational deactivation of CO($v=1$) by inelastic collisions with H_2 and D_2

J. P. Reid and C. J. S. M. Simpson
Physical Chemistry Laboratory, South Parks Road, Oxford OX1 3QZ, United Kingdom

H. M. Quiney
Department of Physics, Clarendon Laboratory, Parks Road, Oxford OX1 3PU, United Kingdom

(Received 11 October 1996; accepted 19 December 1996)

Calculations of the relaxation rate constants, k_{CO-H_2}, for the vibrational deactivation of CO($v=1$) by pH_2 and oH_2 are reported in the temperature range 30 K$<T<$300 K. The CO rotation is treated using the infinite-order sudden (IOS) approximation, while the rotation of H_2 is included using the coupled states (CS) approximation. A near-resonant energy transfer process, in which the H_2 molecule is rotationally excited from $J=2$ to $J=6$ on relaxation of CO($v=1$), is found to account for the experimental observation that $k_{CO-pH_2}/k_{CO-oH_2} > 1$ for this system at temperatures above 80 K. Evidence is presented to suggest that below this temperature, which represents the current lower limit of existing experimental data for the CO($v=1$)-pH_2 system, thermal depopulation of the $J=2$ rotational state in pH_2 reduces the importance of the near-resonant energy transfer process in the determination of k_{CO-pH_2}. For $T \ll 80$ K the ratio $k_{CO-pH_2}/k_{CO-oH_2}<1$ is predicted on the basis of these calculations. At impact energies less than 60 cm^{-1}, the relaxation cross sections increase at a rate which is insufficient to account for the observed upturn in the experimentally determined deactivation rate constants for the CO–nH_2 system below 60 K. Rate constants for the deactivation of CO($v=1$) by oD_2 and pD_2 have also been calculated and compared with experimental data. © *1997 American Institute of Physics.* [S0021-9606(97)01712-1]

I. INTRODUCTION

The vibrational relaxation of CO($v=1$) by collisions with H_2 has been studied extensively, both theoretically[1–11] and experimentally.[12–22] Experimental measurements of the relaxation rate constants for this system have been made using para-H_2 (pH_2)[13,18] and normal-H_2 (nH_2)[17,18] in the temperature range 70 K$<T<$300 K. From these data may be deduced the rate constants for the relaxation of CO($v=1$) by ortho-H_2 (oH_2), revealing, in this temperature range, that pH_2 is a more efficient collision partner than oH_2. More recent measurements[21] of the rate constants for the CO($v=1$)–nH_2 system in the temperature range 35 K$<T<$300 K have shown that the relaxation rate constants increase as the temperature is lowered below 60 K. The theoretical origin of the differences in the relaxation rate constants for the CO($v=1$)–oH_2 and CO($v=1$)–pH_2 systems is this subject of this paper.

The origin of the dependence of the relaxation rate constants on the parity of the H_2 rotational states has been attributed to the near-resonant process

$$\mathrm{CO}(v=1)+\mathrm{H_2}(J=2)\rightarrow\mathrm{CO}(v=0)+\mathrm{H_2}(J=6)+\Delta E \tag{1}$$

involving an exothermic transfer which liberates $\Delta E=83$ cm^{-1} of kinetic energy.[13] The rate constant of this process dominates those of all other mechanisms. In the deactivation of CO($v=1$) by oH_2, the smallest energy mismatch is $\Delta E=520$ cm^{-1}, involving the $(J_{H_2}=1)\rightarrow(J'_{H_2}=5)$ process. This is not a near-resonant process, and makes no significant contribution to the relaxation rate constants in the temperature range 70 K$<T<$300 K. Similar experimental studies of the vibrational relaxation of CO($v=1$) by oD_2 and nD_2 indicate that they are equally efficient as collision partners in the temperature range 100 K$<T<$300 K.[19]

The contribution of process (1) to the Boltzmann-averaged relaxation rate constants is temperature dependent. At sufficiently low temperatures, the contributions from this process to the rate constants are decreased in importance because of the diminished population in the $J=2$ initial rotational state. Extrapolation of the available experimental data suggests that the relaxation rate constants for pH_2 and oH_2 may cross at some temperature in the range 60 K$<T<$80 K. In the limit of low temperatures, the conventional explanation of the ortho–para effect, based on the influence of process (1), is invalid. It is of both theoretical and experimental interest to determine whether such a marked difference between CO($v=1$)–oH_2 and CO($v=1$)–pH_2 persists at low temperatures, and to determine the origin of such an effect if it exists.

Previous theoretical studies of the relaxation of CO($v=1$) by H_2 have failed to provide unequivocal support for the conjecture that process (1) is the principal source of the difference in the experimental rate constants for the pH_2 and nH_2 systems. The rudimentary calculations of Sharma and Kern[3] and the semi-classical calculations of Poulsen and Billing[5] were in qualitative agreement with experiment and confirmed the importance of process (1). The latter of the two calculations employed the interaction potential generated by *ab initio* self-consistent field theory[23,24] augmented by a multipole expansion of the long-range interaction.[25] Baker and Flower[8–10] studied the same system, employing

this same potential and also a potential derived from the electron-gas model.[26] They concluded that process (1) is directly responsible for the observed effect in the rate constants for the CO–pH$_2$ and CO–oH$_2$ systems. However, the more elaborate calculations of Schinke and co-workers,[2,11] for which the interaction potential included dispersion interactions and explicit vibrational coordinate dependence,[1] showed no ortho–para effect in the calculated rate constants for the deactivation of CO($v=1$) by oH$_2$ and pH$_2$.

Further experimental studies of the vibrational deactivation of CO($v=1$) by H$_2$, HD, and D$_2$ at temperatures less than 100 K have revealed that the relaxation rate constants increase at temperatures less than 60 K.[21,22] Similar upturns in the temperature-dependent relaxation rate constants have been observed in theoretical studies of vibrational relaxation in the CO($v=1$)–He and N$_2$($v=1$)–He systems.[27,28] This intriguing behavior is predicted to occur in the temperature range 10–20 K, which is inaccessible to current experimental techniques for systems with such extremely small rate constants having values less than 1×10^{-20} cm^3 molecule^{-1} s^{-1}. Scattering resonances at impact energies of less than 10 cm^{-1} occur because of the influence of the attractive region of the interaction potential,[29,30] and are responsible for the upturns in rate constants for the systems in which isotopes of helium are the collision partners. In the case of the CO–H$_2$ potential, the attractive well is deeper than that which is found in the CO–He and N$_2$–He systems (see for example Refs. 31–33) and could lead to resonances in the scattering cross sections at higher impact energies, which would have a more pronounced effect on the relaxation rate constants at experimentally accessible temperatures. A detailed study of the CO–H$_2$ system at low impact energies is required if the validity of these conjectures is to be established.

Vibrational energy transfer calculations are demanding tests of the quality of intermolecular potentials. A degree of freedom is introduced by the vibrational coordinate dependence of the diatomic molecule whose energy is transferred in the collision. At most experimentally accessible temperatures, the Boltzmann average of the relaxation cross-section samples contributions involving both high and low impact energies. This necessitates the use of as accurate an interaction potential as possible in both the repulsive and attractive regions of the potential.

In this article, we investigate the theoretical origin of the pronounced ortho–para effect in the CO–H$_2$ system, and extend the calculations to study vibrational relaxation in the CO($v=1$)–D$_2$ system. Despite its known limitations,[11,31] the CO($v=1$)–H$_2$ interaction potential used by Schinke and co-workers remains the only published *ab initio* surface to include vibrational coordinate dependence, and is adopted here.

The potential energy surface used in this work is presented in Sec. II, followed by a discussion of the computational aspects of our inelastic scattering calculations in Sec. III. The numerical results of these calculations are presented in Sec. IV, and are discussed and compared with experiment in Sec. V. This article concludes with Sec. VI, which summarizes our findings.

II. POTENTIAL ENERGY SURFACE

The potential energy interaction surface presented by Schinke and co-workers[1,2] was calculated at the self-consistent field (SCF) level of approximation. The H$_2$ molecule was assumed to be a rigid rotor, and long-range interactions were included by damped dispersion terms. The interaction energies were calculated at two H$_2$ orientation angles, nine CO orientation angles, and three CO bond lengths. It was found that the CO–H$_2$ interaction energy was almost independent of the twist angle, φ, which is measured with respect to an axis chosen to be the line of intermolecular separation. All points on the surface at nonequilibrium bond lengths were calculated at $\varphi=0$, within which model one may assume the conservation of the axial components of angular momentum, j_z, for each of the rotors on collision. This greatly simplifies the dynamics of the collisional process if both rotors are treated at the coupled-states (CS) level of approximation.

The interaction potential is expanded in the form

$$V(R,r,\gamma_1,\gamma_2)=\sum_{k,\lambda_1,\lambda_2} V^k_{\lambda_1,\lambda_2}(R)P_{\lambda_1}(\cos\ \gamma_1) \times P_{\lambda_2}(\cos\ \gamma_2)(r-r_e)^k, \tag{2}$$

where $0\leqslant k\leqslant 2$, $0\leqslant\lambda_1\leqslant 8$, and $\lambda_2=0,2$. The subscript of 1 refers to the CO molecule and the subscript of 2 refers to H$_2$. The variable R is the separation between the centers of mass of CO and H$_2$, r is the CO bond length which has an equilibrium value of r_e, and $P_l(x)$ is a Legendre polynomial. The calculation of the expansion coefficients, $V^k_{\lambda_1,\lambda_2}(R)$, which are used to calculate the potential coupling matrix elements for the scattering calculation, are determined by the following method. The SCF interaction energies are split into short-range repulsive interactions and the dipole–quadrupole and quadrupole–quadrupole interactions of the CO and H$_2$ molecules. The electrostatic interactions are given below with $V_{\mathrm{d-q}}$ denoting the dipole–quadrupole interaction and $V_{\mathrm{q-q}}$ denoting the quadrupole-quadrupole interaction:[34]

$$V_{\mathrm{d-q}}=\frac{3}{2}\frac{\mu_{\mathrm{CO}}\Theta_{\mathrm{H_2}}}{R^4}(\cos\ \gamma_1(3\cos^2\ \gamma_2-1) -2\sin\ \gamma_1\sin\ \gamma_2\cos\ \gamma_1\cos\ \gamma_2\cos\ \phi), \tag{3}$$

$$V_{\mathrm{q-q}}=\frac{3}{4}\frac{\Theta_{\mathrm{CO}}\Theta_{\mathrm{H_2}}}{R^5}(1-5\cos^2\ \gamma_1-5\cos^2\ \gamma_2 -17\cos^2\ \gamma_1\cos^2\ \gamma_2+2\sin^2\ \gamma_1\sin^2\ \gamma_2\cos^2\ \phi -16\sin\ \gamma_1\sin\ \gamma_2\cos\ \gamma_1\cos\ \gamma_2\cos\ \phi). \tag{4}$$

The r-dependent dipole and r-dependent quadrupole moments of CO[35,36] are denoted by μ_{CO} and Θ_{CO}, respectively, and $\Theta_{\mathrm{H_2}}$ denotes the r-independent quadrupole moment of H$_2$,[37] with this collision partner treated as a rigid rotor. The electrostatic interactions were subtracted from the SCF data

TABLE I. Coefficients for the fit of the repulsive wall of the H_2–CO potential.

H_2 orientation, γ_2	CO orientation, γ_1								
	0	22.5	45	67.5	90	112.5	145	167.5	180
				$r_{CO}=1.898\ a_0$					
	33.126[a]	22.724	13.588	12.369	17.238	25.960	41.019	60.414	73.103
0	−4.374	−3.002	−1.765	−1.552	−2.138	−2.870	−2.849	−3.447	−3.366
	1.152	1.122	1.141	1.273	1.433	1.530	1.613	1.632	1.655
	41.488	21.423	10.700	11.147	17.004	20.476	25.695	37.091	45.341
90	−4.681	−2.601	−1.326	−1.332	−1.850	−2.487	−3.456	−5.119	−6.248
	1.249	1.152	1.147	1.317	1.499	1.502	1.460	1.456	1.466
				$r_{CO}=2.132a_0$					
	42.348	24.536	12.592	11.495	14.918	19.838	30.197	49.433	65.002
0	−5.345	−3.124	−1.557	−1.299	−1.909	−2.680	−3.855	−5.975	−7.545
	1.173	1.115	1.122	1.283	1.394	1.413	1.430	1.460	1.493
	47.137	19.403	8.927	9.576	15.862	22.685	29.389	44.105	55.464
90	−5.523	−2.452	−1.155	−1.215	−1.678	−2.061	−3.423	−5.534	−7.001
	1.229	1.094	1.091	1.273	1.482	1.562	1.502	1.491	1.504
				$r_{CO}=1.898a_0$					
	67.099	21.244	11.662	10.479	13.839	17.850	27.235	46.275	67.591
0	−7.804	−2.940	−1.428	−1.162	−1.797	−2.522	−3.712	−6.017	−8.404
	1.272	1.040	1.102	1.268	1.375	1.374	1.383	1.417	1.472
	82.631	17.444	7.869	8.555	15.062	23.260	30.482	46.740	26.907
90	−8.455	−2.260	−1.042	−1.124	−1.592	−1.594	−3.281	−5.600	−3.254
	1.359	1.053	1.056	1.242	1.469	1.594	1.516	1.503	1.391

[a]The three numbers for each orientation correspond to the a, b, and c coefficients, respectively, of Eq. (5).

and the remaining repulsive interaction energies fitted, for each set of orientation angles and bond length, to the form

$$V(R,r,\gamma_1,\gamma_2)=(a+bR)\exp(-cR), \tag{5}$$

where the coefficients a, b, and c are presented in Table I. This simple form was chosen to minimize unphysical oscillations in the fitted potential.

In order to evaluate the expansion coefficients, $V^k_{\lambda_1,\lambda_2}(R)$, the repulsive interaction energy is calculated at each CO bond length and for each set of orientation angles. The electrostatic interaction arising from the dipole–quadrupole and quadrupole–quadrupole interactions is added to this using the experimental value of the dipole moment of CO[36] and Eqs. (3) and (4).

For ease of comparison with previous studies, we have adopted the damped dispersion interaction energy of Schinke and co-workers, which is an asymptotic expansion with leading term R^{-6}, and which is independent of r. The damping function used for the dispersion is given by

$$f(R)=\exp[-\gamma(D/R-1)^2] \quad R\leqslant D, \quad f(R)=1 \quad R>D, \tag{6}$$

with $D=4.46$ Å and $\gamma=6$. The dispersion energy is calculated at each set of orientation angles and the repulsive, electrostatic, and dispersion energies combined. From the angular and vibrational coordinate dependence of $V(R,r,\gamma_1,\gamma_2)$ it is then possible to calculate the expansion coefficients, $V^k_{\lambda_1,\lambda_2}(R)$.

Based on a comparison of Fig. 10 in Ref. 1, our vibrationally elastic coupling functions, $V^0_{\lambda_1,\lambda_2}(R)$, are indistinguishable from those of Schinke and co-workers. Although insufficient detail exists for a direct comparison of the inelastic functions, they are qualitatively similar to those obtained from the interaction surface of Thomas, Kraemer, and Diercksen[38] and Schinke and Diercksen[39] for the CO–He system.

More accurate elastic interaction surfaces exist which indicate an anisotropy of the attractive well different to that of the surface used in the present study.[31] However, we regard the surface as sufficiently accurate for its present application because we are concerned mainly with relaxation rate constants which depend on moderately high impact energies. The surface is clearly inadequate for a detailed study of low-energy rotational resonances which were the subject of our recent investigations of the CO–He and N_2–He systems.[27,28] The most significant restriction of the present surface is the low-order expansion of the potential in the variable γ_2, which limits the accuracy with which coupling matrix elements of the near-resonant interaction process (1) can be evaluated. This expansion effectively limits direct coupling of the initial and final rotational states of H_2 to $\Delta J=\pm 2$, though indirect couplings due to oblique collisions are still allowed.

III. SCATTERING CALCULATIONS

The calculations presented in this paper were performed by applying the coupled states approximation to the rotation of H_2 and the infinite order sudden approximation to the rotation of CO. These dynamical approximations are well

documented[40] and are not discussed further here. The CS-IOS formulation of the diatom–diatom collisional process is described in the earlier papers of Schinke and co-workers.[1,2]

The scattering calculations were performed using the molecular scattering program MOLSCAT[41] and the coupled equations were solved using the hybrid log-derivative propagator of Manolopoulos and Alexander.[42] Convergence of the scattering cross sections was ensured to within 1% with respect to the propagator step size, the starting separation for propagation, which was well within the nonclassical region, and the maximum propagation separation of 30 Å. Convergence with respect to the basis set size was also ensured, again to well within 1%. The molecular constants for the rotation of H_2 (Ref. 43) and the basis sets employed are given in Table II. The vibrational constants used[43] for CO were $\omega_e=2169.814\ \mathrm{cm}^{-1}$ and $\omega_e x_e=13.288\ \mathrm{cm}^{-1}$.

More closed channels were required for the CO–D_2 scattering calculations, presumably as a result of the smaller magnitude of the scattering cross sections which are more susceptible to small changes in the convergence of the basis set.

Numerical tests were performed to ensure that the calculations were converged with respect to the maximum angular momentum, $L_{\max}$, included in the partial wave expansion. Contributions from partial waves to $L_{\max}=38$ were required for low and intermediate impact energies, E_{Kin}, while contributions to $L_{\max}=58$ were required for impact energies greater than 1500 cm^{-1}. In all cases, the calculation was initiated at $L=2$ and all partial waves in steps of 4 were considered with the resulting cross section multiplied by a factor of 4.

The scattering calculations were performed at the angles $\gamma_1=n\pi/8$, where $n=0,1,\cdots 8$ which correspond to the orientation angles of CO for which the potential has been evaluated. The IOS average of the relaxation cross section over the CO impact angle[40] was then performed according to the equation

$$\sigma(v_{\mathrm{CO}}=1,J_{\mathrm{H_2}}\rightarrow v_{\mathrm{CO}}=0,J'_{\mathrm{H_2}};E_{\mathrm{Kin}}) = \int_0^{\pi}\sigma(v_{\mathrm{CO}}=1,J_{\mathrm{H_2}}\rightarrow v_{\mathrm{CO}}=0,J'_{\mathrm{H_2}};\gamma_1,E_{\mathrm{Kin}}) \times\sin(\gamma_1)d\gamma_1. \quad (7)$$

Calculations were performed at up to 23 impact energies in the range 5–2000 cm^{-1} in order to obtain accurate thermally averaged rate constants from 30 to 300 K. An accurate characterization of the cross sections below an impact energy of 80 cm^{-1} was essential in order to obtain accurate low temperature rate constants requiring up to 14 impact energies. Rate constants were calculated by first summing the state-to-state relaxation cross sections over the final rotational state of H_2,

$$\sigma_{\mathrm{CS}}(v_{\mathrm{CO}}=1,J_{\mathrm{H_2}}\rightarrow v_{\mathrm{CO}}=0;E_{\mathrm{Kin}}) = \sum_{J'_{\mathrm{H_2}}}\sigma_{\mathrm{CS}}(v_{\mathrm{CO}}=1,J_{\mathrm{H_2}}\rightarrow v_{\mathrm{CO}}=0,J'_{\mathrm{H_2}};E_{\mathrm{Kin}}). \quad (8)$$

TABLE II. Molecular constants and basis set data for the H_2(CS)–CO(IOS) systems.

	CO–H_2 system	CO–D_2 system
Rotational constant	Constants for the H_2 partner	
B_0	59.334 cm^{-1}	29.904 cm^{-1}
D_0	0.047 cm^{-1}	0.011 cm^{-1}
Vibrational state	para-spin isomer	
$v_{\mathrm{CO}}=0$	$J=0,2,4,6$	$J=1,3,5,7,9,11,13,15$
$v_{\mathrm{CO}}=1$	$J=0,2,4,6$	$J=1,3,5,7,9,11,13,15$
$v_{\mathrm{CO}}=2$	$J=0,2,4$	$J=1,3,5,7,9$
	ortho-spin isomer	
$v_{\mathrm{CO}}=0$	$J=1,3,5,7$	$J=0,2,4,6,8,10,12,14$
$v_{\mathrm{CO}}=1$	$J=1,3,5,7$	$J=0,2,4,6,8,10,12,14$
$v_{\mathrm{CO}}=2$	$J=1,3,5$	$J=0,2,4,6,8$

These cross sections were then averaged over the kinetic energy distribution to give rate constants for relaxation from specific initial H_2 rotational states,

$$k_{\mathrm{CS}}(v_{\mathrm{CO}}=1,J_{\mathrm{H_2}}\rightarrow v_{\mathrm{CO}}=0;T) = \left(\frac{8}{\pi\mu(k_BT)^3}\right)^{1/2}\int_0^{\infty}\sigma_{\mathrm{CS}}(v_{\mathrm{CO}}=1,J_{\mathrm{H_2}}\rightarrow v_{\mathrm{CO}}=0;E_{\mathrm{Kin}}) \times\exp(-E_{\mathrm{Kin}}/k_BT)E_{\mathrm{Kin}}dE_{\mathrm{Kin}}. \quad (9)$$

Rate constants for the deactivation of CO ($v=1$) by para- and ortho-H_2 were calculated independently by weighting the rate constants from the specific initial rotational levels, assuming a Boltzmann distribution for their populations. To obtain rate constants for $n\mathrm{H_2}$ and $n\mathrm{D_2}$, rate constants were weighted according to the ratios of the ortho- and para-species given by nuclear spin statistics, i.e., 3:1 of $o\mathrm{H_2}$ to $p\mathrm{H_2}$ and 2:1 of $o\mathrm{D_2}$ to $p\mathrm{D_2}$.

IV. RESULTS

The CO–H_2 and CO–D_2 results are presented separately.

A. The CO–H_2 system

Calculated cross sections are presented in Tables III, IV, and V and in Fig. 1 for the vibrational deactivation of CO by H_2 in an initial rotational state of $J_{\mathrm{H_2}}=0$, 1, and 2, respectively. The cross sections are given in the form of state-to-state contributions in order that a meaningful comparison can be made with the work of Schinke and co-workers.[2,11] The cross sections summed over final rotational states are found to be a factor of approximately 4 lower than those calculated by Schinke and co-workers for the collisional process from an initial state of $J_{\mathrm{H_2}}=0$, a factor of between 2 and 3 low for the collisional process from an initial state of $J_{\mathrm{H_2}}=1$, and between a factor of 8 high at low impact energies and a factor of 2 low at high impact energies for the collisional process originating from an initial state of $J_{\mathrm{H_2}}=2$.

The state-to-state breakdown of cross sections reveals significant differences between the present calculations and

TABLE III. Energy dependence of the IOS averaged vibrational deactivation cross sections $\sigma(v_{CO}=1, j_{H_2}=0 \rightarrow v_{CO}=0, j'_{H_2})$ (in Å^2).

Kinetic energy/cm^{-1}	j'_{H_2} 0	2	4	6	$\Sigma\sigma(j_{H_2}=0)$
5	0.346(−6)	0.460(−6)	0.184(−5)	-	0.265(−5)
10	0.101(−6)	0.146(−6)	0.532(−6)	-	0.778(−6)
15	0.813(−7)	0.116(−6)	0.444(−6)	-	0.642(−6)
20	0.790(−7)	0.119(−6)	0.389(−6)	-	0.587(−6)
30	0.730(−7)	0.106(−6)	0.366(−6)	-	0.544(−6)
42	0.717(−7)	0.100(−6)	0.364(−6)	-	0.536(−6)
50	0.707(−7)	0.978(−7)	0.351(−6)	-	0.520(−6)
60	0.720(−7)	0.993(−7)	0.351(−6)	-	0.522(−6)
87	0.835(−7)[a]	0.112(−6)[a]	0.389(−6)[a]	-	0.584(−6)[a]
	0.113(−5)	0.792(−6)	0.665(−7)	-	0.199(−5)
242	0.269(−6)	0.313(−6)	0.932(−6)	-	0.151(−5)
	0.292(−5)	0.266(−5)	0.159(−6)	-	0.574(−5)
457	0.109(−5)	0.112(−5)	0.251(−5)	0.347(−6)	0.506(−5)
	0.880(−5)	0.851(−5)	0.409(−6)	0.238(−8)	0.177(−4)
687	0.349(−5)	0.330(−5)	0.539(−5)	0.122(−5)	0.134(−4)
	0.240(−4)	0.205(−4)	0.107(−5)	0.282(−7)	0.456(−4)
907	0.855(−5)	0.763(−5)	0.940(−5)	0.251(−5)	0.281(−4)
	0.563(−4)	0.404(−4)	0.263(−5)	0.100(−6)	0.994(−4)
1132	0.183(−4)	0.157(−4)	0.148(−4)	0.434(−5)	0.531(−4)
	0.115(−3)	0.703(−4)	0.582(−5)	0.248(−6)	0.191(−3)
1357	0.351(−4)	0.292(−4)	0.214(−4)	0.675(−5)	0.923(−4)
	0.215(−3)	0.115(−3)	0.119(−4)	0.513(−6)	0.342(−3)
1557	0.580(−4)	0.473(−4)	0.283(−4)	0.945(−5)	0.143(−3)
	0.355(−3)	0.162(−3)	0.221(−4)	0.933(−6)	0.540(−3)
2057	0.164(−3)	0.130(−3)	0.499(−4)	0.189(−4)	0.363(−3)
	0.103(−2)	0.446(−3)	0.794(−4)	0.281(−5)	0.156(−2)
2357	0.274(−3)	0.214(−3)	0.666(−4)	0.268(−4)	0.581(−3)

[a]The first number of each pair refers to the present calculation and the second number to the calculation of Schinke and co-workers (Ref. 11).

those of Schinke and co-workers. Rotationally elastic cross sections calculated in the present study, $\Delta J_{H_2}=0$, are smaller than those of Schinke and co-workers by an order of magnitude at impact energies up to 1000 cm^{-1}. The rotationally inelastic cross sections in the present study for the $\Delta J_{H_2}= \pm 2$ processes are also smaller than those calculated by Schinke and co-workers by an order of magnitude. The rotationally inelastic nonresonant cross sections for the $\Delta J_{H_2}=4$ processes are up to an order of magnitude larger than those calculated by Schinke and co-workers. In all cases, the discrepancy between the present calculation and the calculation of Schinke and co-workers becomes less pronounced at the highest impact energies considered.

The most notable discrepancy arises in comparing the cross sections for the near-resonant $\Delta J_{H_2}=4$ process (1), the $J_{H_2}=2 \rightarrow 6$ transition in H_2. For this process, the present calculation yields cross sections which are between a factor of 20 and 75 higher than those from the calculation of Schinke and co-workers over the energy range 100–1700 cm^{-1}. The near-resonant effect is found from this study to have a scattering cross section two orders of magnitude larger than any other at the lowest of impact energies, although its influence has diminished to one of comparable deactivating efficiency by 2000 cm^{-1}. The dependence of this scattering cross section on impact energy is found to be very weak in comparison to the energy dependence for the nonresonant process. For this process the predominant angular contributions to the IOS averaged scattering cross sections come from oblique impacts in the region 10°–60° (the C end) and 150°–180° (the O end) with the most probable angle for energy transfer shifting to a more oblique angle with increase in impact energy.

An upturn in the scattering cross sections is apparent at impact energies below 50 cm^{-1}, with broad resonances observed in the cross sections.

Thermally averaged rate constants are presented in Table VI for ortho- and para-H_2 and in Table VII for normal-H_2. Comparison with experiment[18,20] is made where possible. Table VII also compares the calculated para-/ortho-H_2 ratio with the experimental ratio.[18] These results are also presented in Figs. 2, 3, and 4, with the complete set of calculated rate constants shown in Fig. 5.

B. The CO–D_2 system

Cross sections are presented in Tables VIII and Tables IX for the vibrational deactivation of CO by D_2 in an initial rotational state of $J=0$ and 1, respectively. Unlike the near-resonant collisional process in the CO–H_2 system, the process

TABLE IV. Energy dependence of the IOS averaged vibrational deactivation cross sections $\sigma(v_{CO}=1, j_{H_2}=1 \rightarrow v_{CO}=0, j'_{H_2})$ (in Å^2).

Kinetic energy/cm^{-1}	j'_{H_2} 1	3	5	7	$\Sigma\sigma(j_{H_2}=1)$
8	0.148(−6)	0.387(−6)	0.548(−5)	-	0.601(−5)
10	0.131(−6)	0.311(−6)	0.527(−5)	-	0.572(−5)
13	0.120(−5)	0.268(−5)	0.475(−5)	-	0.514(−5)
15	0.110(−6)	0.265(−6)	0.469(−5)	-	0.507(−5)
18	0.107(−6)	0.257(−6)	0.394(−5)	-	0.430(−5)
20	0.108(−6)	0.279(−6)	0.367(−5)	-	0.406(−5)
23	0.110(−6)	0.281(−6)	0.360(−5)	-	0.399(−5)
25	0.105(−6)	0.259(−6)	0.377(−5)	-	0.414(−5)
33	0.103(−6)	0.242(−6)	0.394(−5)	-	0.429(−5)
36	0.100(−6)	0.239(−6)	0.372(−5)	-	0.405(−5)
43	0.950(−7)	0.212(−6)	0.340(−5)	-	0.370(−5)
51	0.938(−7)	0.208(−6)	0.327(−5)	-	0.357(−5)
63	0.955(−7)	0.212(−6)	0.320(−5)	-	0.351(−5)
88	0.110(−6)[a]	0.233(−6)[a]	0.344(−5)[a]	-	0.378(−5)[a]
	0.143(−5)	0.463(−5)	0.243(−6)	-	0.630(−5)
240	0.338(−6)	0.586(−6)	0.631(−5)	-	0.724(−5)
	0.334(−5)	0.117(−4)	0.511(−6)	-	0.155(−4)
455	0.132(−5)	0.194(−5)	0.128(−4)	-	0.160(−4)
685	0.415(−5)	0.531(−5)	0.220(−4)	-	0.314(−4)
	0.275(−4)	0.580(−4)	0.207(−5)	-	0.876(−4)
905	0.109(−4)	0.116(−4)	0.327(−4)	-	0.544(−4)
1130	0.216(−4)	0.226(−4)	0.454(−4)	-	0.895(−4)
1355	0.414(−4)	0.398(−4)	0.596(−4)	0.871(−7)	0.141(−3)
1555	0.686(−4)	0.618(−4)	0.735(−4)	0.243(−7)	0.204(−3)
2055	0.195(−3)	0.154(−3)	0.113(−3)	0.135(−5)	0.464(−3)
2540	0.431(−3)	0.312(−3)	0.158(−3)	0.410(−5)	0.905(−3)

[a]The first number of each pair refers to the present calculation and the second number to the calculation of Schinke and co-workers (Ref. 11).

$$CO(v=1)+D_2(J=0)\rightarrow CO(v=0)+D_2(J=8)+\Delta E = 49.3\ \text{cm}^{-1} \quad (10)$$

is not found to have an enhanced cross section in comparison with those for other collisional processes. No previous theoretical calculations exist with which to make a comparison. Again, as for the CO–H_2 system, an upturn in collision cross sections is apparent at impact energies below 50 cm^{-1}.

Thermally averaged rate constants are presented in Table X for both ortho- and para-D_2, and for normal-D_2 and the

TABLE V. Energy dependence of the IOS averaged vibrational deactivation cross sections $\sigma(v_{CO}=1, j_{H_2}=2 \rightarrow v_{CO}=0, j'_{H_2})$ (in Å^2).

Kinetic energy/cm^{-1}	j'_{H_2} 0	2	4	6	$\Sigma\sigma(j_{H_2}=2)$
102	0.483(−8)[a]	0.113(−6)[a]	0.102(−5)[a]	0.119(−3)[a]	0.121(−3)[a]
	0.468(−7)	0.141(−5)	0.117(−4)	0.158(−5)	0.147(−4)
332	0.308(−7)	0.581(−6)	0.367(−5)	0.963(−4)	0.101(−3)
	0.245(−6)	0.513(−5)	0.380(−4)	0.178(−5)	0.452(−4)
552	0.119(−6)	0.204(−5)	0.101(−4)	0.983(−4)	0.111(−3)
	0.891(−6)	0.155(−4)	0.794(−4)	0.209(−5)	0.979(−4)
777	0.351(−6)	0.566(−5)	0.230(−4)	0.105(−3)	0.134(−3)
	0.288(−5)	0.363(−4)	0.155(−3)	0.257(−5)	0.197(−3)
1002	0.855(−6)	0.131(−4)	0.450(−4)	0.115(−3)	0.174(−3)
	0.724(−5)	0.871(−4)	0.251(−3)	0.309(−5)	0.348(−3)
1202	0.168(−5)	0.248(−4)	0.741(−4)	0.127(−3)	0.227(−3)
	0.148(−4)	0.162(−3)	0.324(−3)	0.398(−5)	0.505(−3)
1702	0.651(−5)	0.893(−4)	0.199(−3)	0.163(−3)	0.458(−3)
	0.562(−4)	0.562(−3)	0.550(−3)	0.759(−5)	0.118(−2)
2002	0.125(−4)	0.165(−3)	0.317(−3)	0.189(−3)	0.684(−3)

[a]The first number of each pair refers to the present calculation and the second number to the calculation of Schinke and co-workers (Ref. 11).

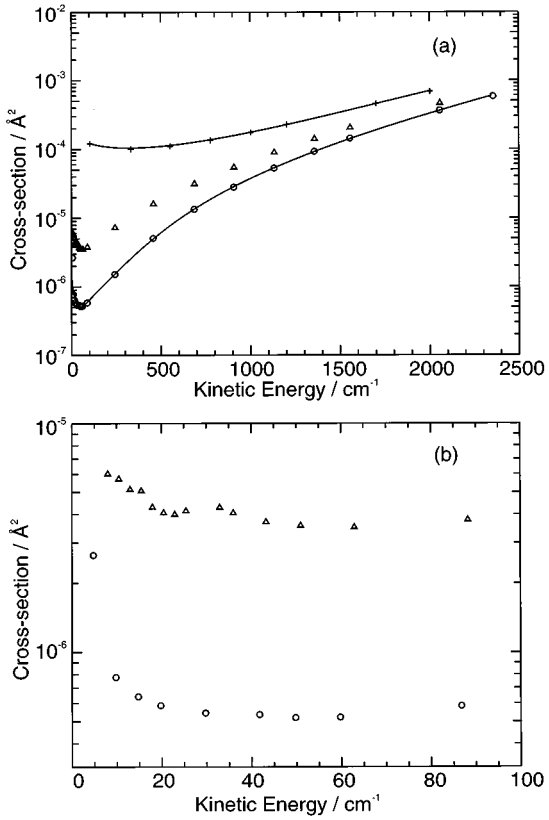

FIG. 1. Cross sections for the vibrational deactivation of CO($v=1$) by $H_2(J)$ summed over all final rotational states of H_2. Initial $H_2(J=0)$: ○; Initial H_2 ($J=1$): △; Initial $H_2(J=2)$: +.

ortho-/para-ratio is shown. A comparison is made with the experimental data.[19,21] Rate constants are also presented in Fig. 6.

V. DISCUSSION

A. CO–H_2

In order to compare directly our *ab initio* calculations of the vibrational relaxation rate constants for the CO–H_2 system with experiment, we note that the rate constants for the CO–oH_2 system can be calculated from those for CO–pH_2 and CO–nH_2 using the relation

$$k_{\mathrm{CO}-o\mathrm{H}_2} = \tfrac{4}{3}(k_{\mathrm{CO}-n\mathrm{H}_2} - \tfrac{1}{3}k_{\mathrm{CO}-p\mathrm{H}_2}).$$

Simpson and co-workers[18] have measured relaxation rate constants for the CO–pH_2 system in the temperature range 80 K$<T<$300 K, and for the CO–nH_2 system[21] in the temperature range 35 K$<T<$300 K, which we use as the primary data against which to assess the accuracy of our theoretical studies. Reference to ''experimental values'' of $k_{\mathrm{CO}-o\mathrm{H}_2}$ should be interpreted as values deduced from $k_{\mathrm{CO}-n\mathrm{H}_2}$ and $k_{\mathrm{CO}-p\mathrm{H}_2}$ using the above relation. The theoretical values of the relaxation rate constants and the available experimental data are presented in Tables VI and VII and Figs. 2–5.

Direct comparison between theoretical and experimental values of the relaxation rate constants for CO–oH_2 and CO–pH_2 systems is currently possible only in the temperature range 80 K$<T<$300 K. The theoretically deduced rate constants for all three systems intersect at a temperature of approximately 120 K, with the values for the $k_{\mathrm{CO}-p\mathrm{H}_2}$ system larger than those for the $k_{\mathrm{CO}-o\mathrm{H}_2}$ system above the intersection temperature, and smaller below the intersection temperature. The experimental data for the $k_{\mathrm{CO}-o\mathrm{H}_2}$ and $k_{\mathrm{CO}-p\mathrm{H}_2}$ systems appear to converge near the lower experimental temperature limit. For all measured temperatures in this range, pH_2 is a more efficient collision partner than nH_2, and consequently oH_2, in the vibrational deactivation of CO ($v=1$). The pH_2/oH_2 ratio deduced from these data is great--est for $T\simeq160$ K, with a value 4.7. As the temperature is increased above this value, the pH_2/oH_2 ratio decreases, presumably because the quantum mechanical selection of the allowed processes enforced by the angular momentum of the H_2 becomes less significant, and the values of the rate constants are dominated by ballistic collisions which depend only on the masses of the colliding particles. A similar be-

TABLE VI. Rate constants for the vibrational deactivation of CO ($v=1$) by para- and ortho-H_2.

	para-H_2			ortho-H_2		
Temperature/K	$k_{\mathrm{Expt.}}$	k_{Theory}	$k_{\mathrm{Theory}}/k_{\mathrm{Expt.}}$	$k_{\mathrm{Expt.}}$	k_{Theory}	$k_{\mathrm{Theory}}/k_{\mathrm{Expt.}}$
30	-	4.06(−18)	-	-	2.60(−17)	-
35	-	4.13(−18)	-	-	2.68(−17)	-
40	-	4.28(−18)	-	-	2.78(−17)	-
50	-	4.85(−18)	-	-	3.06(−17)	-
60	-	5.97(−18)	-	-	3.44(−17)	-
70	-	8.17(−18)	-	-	3.89(−17)	-
80	2.5(−17)	1.23(−17)	0.49	1.9(−17)	4.41(−17)	2.3
90	4.3(−17)	1.93(−17)	0.45	2.2(−17)	4.99(−17)	2.3
100	5.5(−17)	3.04(−17)	0.55	2.6(−17)	5.62(−17)	2.2
120	1.1(−16)	6.74(−17)	0.61	3.2(−17)	7.07(−17)	2.2
160	2.4(−16)	2.05(−16)	0.85	5.1(−17)	1.08(−16)	2.1
200	3.8(−16)	4.05(−16)	1.1	9.9(−17)	1.62(−16)	1.6
250	5.8(−16)	6.96(−16)	1.2	2.0(−16)	2.65(−16)	1.3
290	8.1(−16)	9.49(−16)	1.2	3.1(−16)	3.87(−16)	1.2

TABLE VII. Rate constants for the vibrational deactivation of CO ($v=1$) by normal-H_2 and a comparison of the ortho-/para-hydrogen effect in the deactivation rate constants.

	normal-H_2			para-/-ortho-H_2	
Temperature/K	$k_{\text{Expt.}}$	k_{Theory}	$k_{\text{Theory}}/k_{\text{Expt.}}$	$k_{\text{exp,para}}/k_{\text{exp,ortho}}$	$k_{\text{theory,para}}/k_{\text{theory,ortho}}$
35	2.0(−17)	2.11(−17)	1.1	-	0.15
40	1.8(−17)	2.19(−17)	1.2	-	0.15
50	1.8(−17)	2.42(−17)	1.3	-	0.15
60	1.8(−17)	2.73(−17)	1.5	-	0.17
70	2.0(−17)	3.12(−17)	1.6	-	0.21
80	2.2(−17)	3.62(−17)	1.6	1.3	0.28
90	2.7(−17)	4.23(−17)	1.6	2.0	0.39
100	3.5(−17)	4.98(−17)	1.4	2.1	0.54
120	5.4(−17)	6.98(−17)	1.3	3.4	0.95
160	1.1(−16)	1.32(−16)	1.2	4.7	1.9
200	1.9(−16)	2.22(−16)	1.2	3.8	2.5
250	3.3(−16)	3.73(−16)	1.1	2.9	2.6
290	4.7(−16)	5.27(−16)	1.1	2.6	2.5

haviour is observed in the temperature dependence of the specific heats of $n\text{H}_2$ and $p\text{H}_2$ which converge at high temperatures. On the basis of the experimental results for $k_{\text{CO}-n\text{H}_2}$ and for $k_{\text{CO}-p\text{H}_2}$ down to 80 K, there is a clear indication that below 80 K $k_{\text{CO}-o\text{H}_2}$ is greater than $k_{\text{CO}-p\text{H}_2}$. This is consistent with the general trend observed in the theoretical values of these quantities.

In absolute terms, the agreement between the theoretical and experimental values of the relaxation rate constants is good, particularly for the highest temperatures considered in this range. For these temperatures, the ratio between the experimental and theoretical values of $k_{\text{CO}-p\text{H}_2}$ and $k_{\text{CO}-o\text{H}_2}$ is stable at approximately 1.2, and consequently the calculated ratio $k_{\text{CO}-p\text{H}_2}/k_{\text{CO}-o\text{H}_2}$ is very close to the experimental value of 2.6 at 290 K.

The observed ortho–para effect in the deactivation of the CO ($v=1$)–H_2 system has been attributed to the near-resonant $\Delta J=4$ process defined by (1). It is certainly true that of all the possible relaxation pathways for these systems, the relaxation cross sections due to this process dominate the contributions from all others in the calculation of *thermally averaged* relaxation rate constants above 100 K. On the basis of our theoretical investigations, however, it appears that the attribution of the ortho–para effect to this single resonant process is misleading, particularly when the implication is that the relaxation rate constants for the two systems would be comparable in the absence of this single contribution.

A theoretical appreciation of the nature of the ortho–para effect in the deactivation of CO($v=1$) by H_2 in the temperature range 35 K$<T<$300 K may be obtained if we arbitrarily eliminate the contribution of the near-resonant process (1) to $k_{\text{CO}-p\text{H}_2}$, and calculate a model relaxation rate constant labeled $k'_{\text{CO}-p\text{H}_2}$ (Fig. 7). Across the entire temperature range $k'_{\text{CO}-p\text{H}_2}<k_{\text{CO}-p\text{H}_2}$, with apparent convergence at very high temperatures, as one would expect in a classical limit for which quantum effects are eliminated. At 35 K, however, $k'_{\text{CO}-p\text{H}_2}=k_{\text{CO}-p\text{H}_2}$, revealing a quite different ortho–para effect in this system from the one which has been

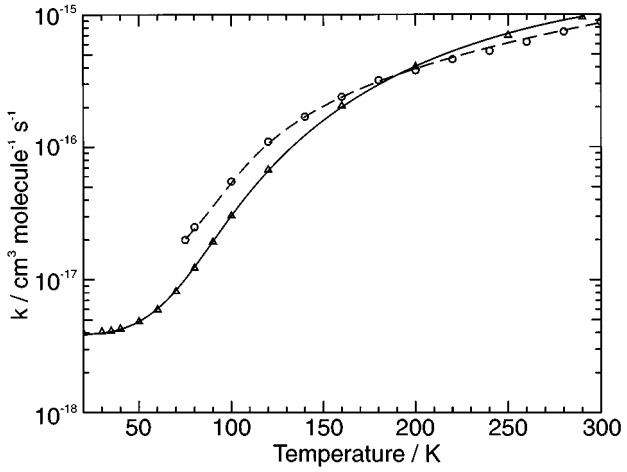

FIG. 2. Rate constants for the vibrational deactivation of CO($v=1$) by para-H_2 The IOS-CS calculation: —, △; Experiment: ––, ○.

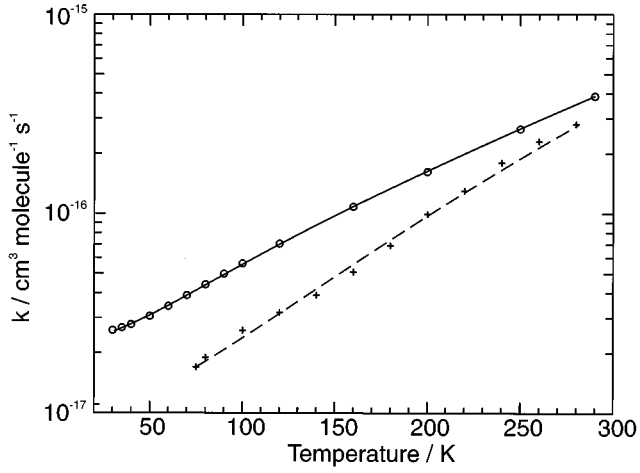

FIG. 3. Rate constants for the vibrational deactivation of CO($v=1$) by ortho-H_2. The IOS-CS calculation: —, ○; Experiment: ––, +.

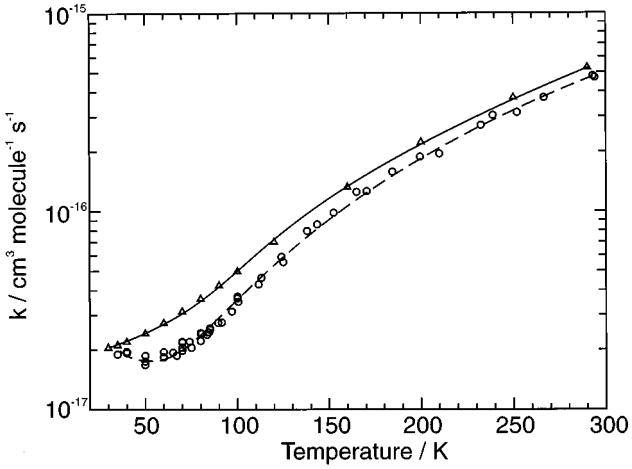

FIG. 4. Rate constants for the vibrational deactivation of CO($v=1$) by normal-H_2. The IOS-CS calculation: —, △; Experiment: ––, ○.

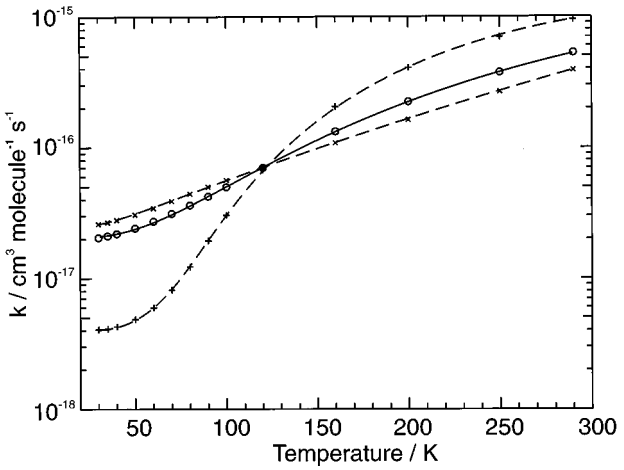

FIG. 5. Comparison of the theoretically calculated rate constants for the vibrational deactivation of CO($v=1$) by para-, ortho-, and normal-H_2. nH_2: —, ○; pH_2: ––, +; oH_2: ––, ×.

observed experimentally in the range 80 K$<T<$300 K.

Superimposed on Fig. 7 are the theoretically determined values of k_{CO-pH_2}, which illustrate dramatically the influence of the process (1) as a function of temperature. At 35 K, the thermal population of the $J=2$ rotational state of H_2 is too small for processes originating in this initial state to make any contribution to the thermally averaged relaxation rate constant. The behavior of the rate constants is determined solely by processes with an initial rotational state of $J=0$. As the temperature is increased, the theoretical values of k_{CO-pH_2} grow exponentially as the thermal population of the $J=2$ rotational state of H_2 increases, until it becomes the dominant effect, and reverses the efficiency of pH_2 and oH_2 as collision partners in the vibrational deactivation of CO ($v=1$).

These theoretical results indicate that in the temperature range covered by experiment, 80 K$<T<$300 K, the ortho–para effect should not be thought of as being solely due to the enhancement of k_{CO-pH_2} by the near-resonant process (1). In fact, the systems CO–oH_2 and CO–pH_2 have few dynamical features in common in this temperature range. The symmetry constraints imposed by the two spin isomers of hydrogen ensure that vibrational relaxation in the two systems involve mutually exclusive energy transfer pathways. It is only in the limit of temperatures far higher than those studied in this paper that the distinction between the spin isomers is lost. It is interesting that a similar ortho-/para-H_2 difference occurs in the deactivation rate constants of the

TABLE VIII. Energy dependence of the IOS averaged vibrational deactivation cross sections $\sigma(v_{CO}=1, j_{D_2}=0 \rightarrow v_{CO}=0, j'_{D_2})$ (in Å^2).

	j'_{D_2}						
Kinetic energy/cm^{-1}	0	2	4	6	8	10	$\Sigma\sigma(j_{D_2}=0)$
5	0.142(−8)	0.804(−8)	0.671(−9)	0.597(−9)	0.502(−9)	-	0.112(−7)
10	0.377(−9)	0.200(−8)	0.176(−9)	0.349(−9)	0.326(−9)	-	0.323(−8)
15	0.173(−9)	0.721(−9)	0.751(−10)	0.295(−9)	0.310(−9)	-	0.157(−8)
20	0.107(−9)	0.433(−9)	0.563(−10)	0.271(−9)	0.260(−9)	-	0.113(−8)
30	0.924(−10)	0.301(−9)	0.388(−10)	0.277(−9)	0.234(−9)	-	0.944(−9)
40	0.709(−10)	0.205(−9)	0.316(−10)	0.270(−9)	0.232(−9)	-	0.810(−9)
50	0.569(−10)	0.137(−9)	0.292(−10)	0.282(−9)	0.240(−9)	-	0.746(−9)
60	0.671(−10)	0.181(−9)	0.286(−10)	0.304(−9)	0.218(−9)	-	0.799(−9)
70	0.659(−10)	0.178(−9)	0.308(−10)	0.332(−9)	0.225(−9)	-	0.831(−9)
80	0.598(−10)	0.128(−9)	0.292(−10)	0.365(−9)	0.232(−9)	-	0.813(−9)
90	0.667(−10)	0.152(−9)	0.338(−10)	0.400(−9)	0.245(−9)	-	0.898(−9)
240	0.331(−9)	0.527(−9)	0.130(−9)	0.169(−8)	0.729(−9)	-	0.340(−8)
460	0.266(−8)	0.356(−8)	0.679(−9)	0.782(−8)	0.282(−8)	-	0.175(−7)
690	0.140(−7)	0.164(−7)	0.245(−8)	0.243(−7)	0.798(−8)	-	0.651(−7)
900	0.474(−7)	0.503(−7)	0.639(−7)	0.533(−7)	0.172(−7)	-	0.175(−6)
1130	0.143(−6)	0.141(−6)	0.162(−7)	0.106(−6)	0.349(−7)	0.428(−12)	0.441(−6)
1400	0.423(−6)	0.388(−6)	0.441(−7)	0.203(−6)	0.703(−7)	0.197(−10)	0.113(−5)
1600	0.845(−6)	0.745(−6)	0.886(−7)	0.302(−6)	0.110(−6)	0.107(−9)	0.209(−5)
2100	0.351(−5)	0.290(−5)	0.422(−6)	0.654(−6)	0.285(−6)	0.160(−8)	0.777(−5)
2457	0.797(−5)	0.647(−5)	0.110(−5)	0.989(−6)	0.500(−6)	0.583(−8)	0.170(−4)

TABLE IX. Energy dependence of the IOS averaged vibrational deactivation cross sections $\sigma(v_{CO}=1, j_{D_2}=1 \rightarrow v_{CO}=0, j'_{D_2})$ (in Å^2).

Kinetic energy/cm^{-1}	j'_{D_2} 1	3	5	7	9	11	$\Sigma\sigma(j_{D_2}=1)$
5	0.372(−8)	0.522(−8)	0.283(−9)	0.227(−8)	-	-	0.115(−7)
10	0.115(−8)	0.148(−8)	0.149(−9)	0.139(−8)	-	-	0.417(−8)
15	0.580(−9)	0.572(−9)	0.121(−9)	0.138(−8)	-	-	0.266(−8)
20	0.304(−9)	0.314(−9)	0.116(−9)	0.121(−8)	-	-	0.194(−8)
30	0.176(−9)	0.239(−9)	0.113(−9)	0.117(−8)	-	-	0.170(−8)
40	0.136(−9)	0.187(−9)	0.103(−9)	0.109(−8)	-	-	0.152(−8)
50	0.122(−9)	0.132(−9)	0.107(−9)	0.110(−8)	-	-	0.146(−8)
60	0.119(−9)	0.128(−9)	0.114(−9)	0.115(−8)	-	-	0.151(−8)
70	0.110(−9)	0.132(−9)	0.124(−9)	0.122(−8)	-	-	0.159(−8)
80	0.112(−9)	0.113(−9)	0.132(−9)	0.130(−8)	-	-	0.166(−8)
90	0.182(−9)	0.218(−9)	0.146(−9)	0.139(−8)	-	-	0.194(−8)
240	0.481(−9)	0.454(−9)	0.625(−9)	0.421(−8)	-	-	0.577(−8)
460	0.360(−8)	0.298(−8)	0.314(−8)	0.149(−7)	0.969(−11)	-	0.246(−7)
690	0.182(−7)	0.139(−7)	0.106(−7)	0.394(−7)	0.210(−9)	-	0.823(−7)
900	0.600(−7)	0.438(−7)	0.248(−7)	0.790(−7)	0.102(−8)	-	0.209(−6)
1130	0.178(−6)	0.124(−6)	0.525(−7)	0.147(−6)	0.361(−8)	-	0.505(−6)
1400	0.519(−6)	0.345(−6)	0.108(−6)	0.268(−6)	0.111(−7)	-	0.125(−5)
1600	0.103(−5)	0.667(−6)	0.173(−6)	0.392(−6)	0.217(−7)	0.103(−13)	0.228(−5)
2100	0.422(−5)	0.261(−5)	0.489(−6)	0.855(−6)	0.801(−7)	0.108(−10)	0.825(−5)
2457	0.960(−5)	0.580(−5)	0.980(−6)	0.133(−5)	0.165(−6)	0.110(−9)	0.179(−4)

bending mode of CO_2.[44] This has been attributed to the near-resonant process

$$CO_2(01^10)+H_2(J=1)\rightarrow CO_2(00^00)+H_2(J=3)+\Delta E = 80\ \text{cm}^{-1}. \quad (11)$$

The possible existence of a low-temperature ortho–para effect on the relaxation rate constants, and the upturn in the relaxation rate constants which has been observed at temperatures below 60 K for the CO–nH$_2$ system, predicate that the CO–H$_2$ system remains of considerable theoretical and experimental interest.

The theoretical explanation of the observed upturn in relaxation rate constants for the CO–nH$_2$ system at temperatures below 60 K poses a formidable computational challenge. In order for an upturn in the rate constants to be predicted theoretically, the low-energy relaxation cross sections must counteract the damping factor $E\exp(-E/kT)$ when the average over impact energies is taken. Contributions from cross sections for which $E \gg kT$ are strongly suppressed, so that an upturn in the relaxation rate constants can only come from a strong upturn in relaxation cross sections corresponding to $E<kT$. Although an upturn in the relaxation cross section below an impact energy of 60 cm^{-1} is found in the present study (Fig. 1), this upturn is not sufficient to produce the upturn in thermally averaged rate constants which is observed experimentally. The low-energy upturn in the relax-

TABLE X. Rate constants for the vibrational deactivation on CO ($v=1$) by D$_2$.

Temperature/K	n-D$_2$ $k_{Exp.}$	k_{Theory}	$k_{Theory}/k_{Exp.}$	oD$_2$ and pD$_2$ k_{ortho}	k_{para}	k_{ortho}/k_{para}
20	-	7.28(−21)	-	6.36(−21)	9.36(−21)	0.68
30	-	8.20(−21)	-	6.86(−21)	1.11(−20)	0.62
35	6.0(−20)	8.71(−21)	0.15	7.17(−21)	1.21(−20)	0.59
40	5.2(−20)	9.30(−21)	0.18	7.56(−21)	1.31(−20)	0.58
50	5.1(−20)	1.08(−20)	0.21	8.72(−21)	1.53(−20)	0.57
60	5.8(−20)	1.29(−20)	0.22	1.06(−20)	1.79(−20)	0.59
70	6.6(−20)	1.60(−20)	0.24	1.37(−20)	2.11(−20)	0.65
80	7.9(−20)	2.02(−20)	0.26	1.81(−20)	2.50(−20)	0.72
90	1.0(−19)	2.60(−20)	0.26	2.45(−20)	2.98(−20)	0.82
100	1.3(−19)	3.36(−20)	0.26	3.29(−20)	3.61(−20)	0.91
120	2.2(−19)	5.64(−20)	0.26	5.79(−20)	5.50(−20)	1.0
160	7.8(−19)	1.52(−19)	0.19	1.59(−19)	1.42(−19)	1.1
200	1.9(−18)	3.75(−19)	0.20	3.85(−19)	3.67(−19)	1.0
250	6.3(−18)	9.96(−19)	0.16	9.88(−19)	1.04(−18)	0.95
290	1.3(−17)	1.91(−18)	0.15	1.85(−18)	2.08(−18)	0.89

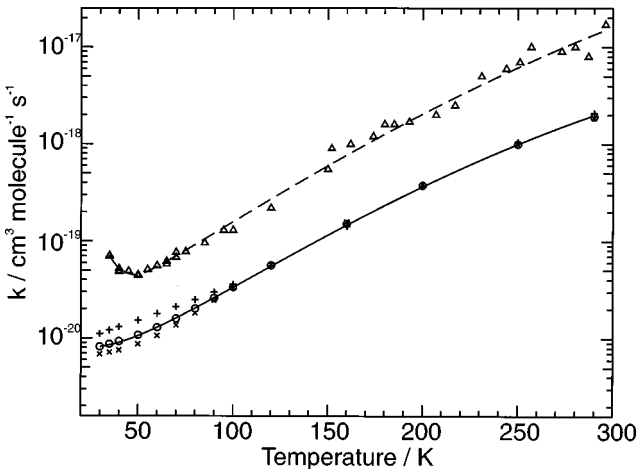

FIG. 6. Rate constants for the vibrational deactivation of CO($v=1$) by para-, ortho-, and normal-D_2. The IOS-CS calculation: nD$_2$: —, ○; pD$_2$: +; oD$_2$: ×. Experiment: ––, △.

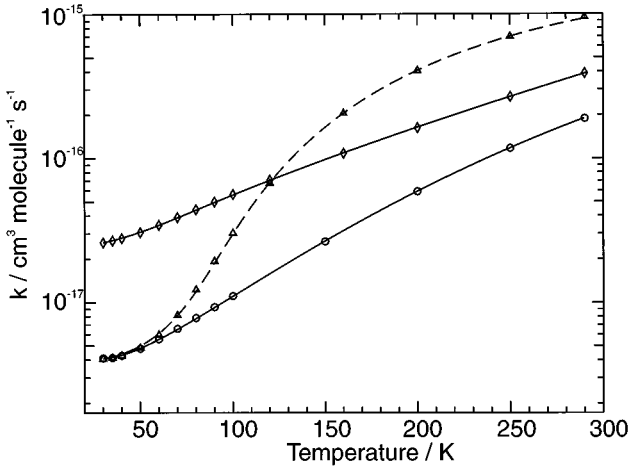

FIG. 7. Comparison of the theoretically calculated rate constants for the vibrational deactivation of CO($v=1$) by para-H_2 with and without the near-resonant $J=2\rightarrow6$ pathway. CO–pH$_2$ without near-resonant pathway: —, ○; CO–pH$_2$ with near-resonant pathway: ––, △; CO–oH$_2$: —, ◆.

ation cross sections generates no upturn in the theoretical relaxation rate constants for the CO–nH$_2$ system, although a change in their curvature is discernible in Fig. 4.

The failure to reproduce the qualitative features of the experimental data at temperatures below 60 K may be due to several factors. The interaction potential used in the present study was not sufficiently accurate to warrant the use of the coupled states approximation in the treatment of the rotation of the CO molecule, since a CS–CS treatment of the rotational coupling for the diatom–diatom system is close to the technical limit of what is currently possible using existing computer codes and computer hardware. It is possible that qualitatively correct behavior of the relaxation rate constants might be obtained simply through the use of a more accurate interaction potential, but such estimates based on the IOS approximation for the treatment of the rotation of CO cannot be regarded as reliable at low temperatures. Our previous studies of vibration relaxation in the CO–He system[45] revealed that a CS treatment is essential if low-energy interactions between the lighter mass projectile and the heavier target molecule are to be modeled correctly. A detailed calculation of this type which employs a more accurate interaction potential than is presently available is essential if a satisfactory theoretical explanation of the temperature dependence of the relaxation rate constants of the CO–H_2 system is to be found.

In comparing the results of the current study with the calculation of Schinke and co-workers we have mentioned above that the breakdown of cross sections into state-to-state contributions is different for the two studies. A number of possible sources for the discrepancy has been investigated without success. The basis set expression used in the present study included the dependence of the rotational energy on centrifugal distortion unlike the earlier study. Schinke and co-workers also used a different value for the range parameter in the damping function although we have used the most reliable value based on the evidence of molecular beam data, as suggested in the initial paper of Schinke and co-workers.[1] In the evaluation of the intermolecular potential we have also included the quadrupole–quadrupole interaction of CO and H_2 and the angular dependence of the electrostatic interactions as given by Eqs. (3) and (4). We have compared the vibrationally elastic coupling terms calculated from the potential fit used in this paper with those calculated and presented in the paper of Schinke and co-workers and have found good agreement. No similar comparison can be made between the vibrationally inelastic terms calculated in the two studies as no angular dependence is presented for these

TABLE XI. Cross sections for the deactivation of CO ($v=1$) by H_2: Comparison of calculations on the Schinke and Poulsen potential energy surfaces at an impact energy of 210 cm^{-1} and an initial J_{H_2} of 2.

Calculation	J'_{H_2} 0	2	4	6	$\Sigma_{J'_{H_2}}\sigma(j'_{H_2})$
This calculation	0.115(−7)[a]	0.234(−6)	0.182(−6)	0.102(−4)	0.106(−4)
	0.43	0.32	0.20	0.45	0.43
Schinke's calculation	0.112(−6)	0.275(−5)	0.214(−4)	0.178(−5)	0.260(−4)
	4.2	3.7	23.5	12.6	1.1
CS-IOS on Poulsen surface	0.268(−7)	0.736(−6)	0.908(−6)	0.225(−4)	0.241(−4)

[a]The second number of each pair is the ratio of the calculation to that on the Poulsen surface.

coupling terms in the paper of Schinke and co-workers. This is most unfortunate as it might reveal the source of the discrepancy between the two calculations. Our study, however, is in agreement with that of Schinke and co-workers[11] on the Poulsen surface.[5] A comparison of the three calculations is presented in Table XI. It is also instructive to compare the current calculation with those of Baker and Flower.[8–10] The magnitude of the near-resonant cross section [process (1)] obtained by the present calculation, as well as being very closely in agreement with that obtained by Schinke and co-workers on the Poulsen surface, is also very closely in agreement with that obtained by Baker and Flower.

We conclude that our calculation, although inconsistent with the calculation of Schinke and co-workers on this potential energy surface, is consistent with experimental measurement and also with previous calculations on a second potential energy surface. Schinke and co-workers concluded that there was no ortho-/para-H_2 effect in contrast to the present study and those of Poulsen and Billing, as well as the experimental evidence.

B. The CO–D_2 system

Several studies have been performed on the inelastic rotational scattering of CO and D_2,[46–49] although this is the first to consider the vibrational deactivation of CO($v=1$) by D_2. The balance of the reduction of energy mismatch of the collisional process by the rotational excitation of D_2 in the final state and the preference for minimal ΔJ change in D_2 are the two most important factors. An example of is found in considering the cross sections originating from $J_{D_2}=0$. Two maxima are seen in the final state distribution of cross sections at $J'_{D_2}=2$ and 6, the two processes having energy mismatches of 1964.2 and 907.4 cm^{-1}, respectively.

The calculated rate constants are an underestimate of those measured experimentally[19,21] by as much as a factor of 6. The validity of the IOS approximation has been found to be dependent on the reduced mass of the collision pair.[45] This is one possible source for the larger discrepancy between theory and experiment for this system than was observed for the CO–H_2 system. Further, the lack of direct coupling between J states for $\Delta J \geqslant 4$ will be even more influential on the scattering cross sections for the CO–D_2 system than for the H_2 system. Larger changes in the rotational quantum number of D_2 will be possible with its rotational constant having a much smaller value than that for H_2. The lack of high order Legendre terms in the potential expansion will limit the accuracy with which cross sections for the near-resonant processes $J_{D_2}=0\rightarrow 8$ ($\Delta E=49.3$ cm^{-1}) and $J_{D_2}=3\rightarrow 9$ (-99 cm^{-1}) can be calculated.

No difference in the theoretical values of k_{CO-oD_2} and k_{CO-pD_2} is found at temperatures over 100 K and this is in agreement with experiment.[19] However, below 90 K an ortho-/para-D_2 difference of up to a factor of 2 is predicted theoretically with relaxation being more efficient from para-D_2 (odd rotational states) than from ortho-D_2 (even rotational states). With $J_{D_2}=1$ and 3 being the most populated states of pD_2 at low temperatures, the comparison of cross sections originating from $J_{D_2}=0$, 1, 2, and 3 suggests that the ortho-/para-D_2 difference found below 90 K may be attributed to the $J_{D_2}=1\rightarrow 7$ ($+564.1$ cm^{-1}) process and the $J_{D_2}=3\rightarrow 7$ ($+861.8$ cm^{-1}) process. This may be easily explained by considering the energy mismatches of the relevant relaxation pathways, with this being the dominant influence on collision cross sections at low impact energies. The $J_{D_2}=0\rightarrow 8$ near-resonant process ($+49.3$ cm^{-1}) is too large a ΔJ_{D_2} process to be modeled accurately by this potential and consequently its influence on the rate constants in reality is impossible to judge. This is also true when considering the other near resonant process, $J_{D_2}=3\rightarrow 9$.

Our reservations regarding the reliability of the IOS approximation in the treatment of the rotation of the CO molecule, and the inaccuracy of the interaction potential, are as pertinent to this system as they were to CO–H_2. Although a marked upturn in the relaxation cross sections at low impact energies is found, which is consistent with the observed upturn in the rate constants at low temperatures, the theoretical values of the rate constants do not exhibit the qualitative features of the experimental data. From this one may deduce only that the low-energy cross sections do not increase sufficiently in the limit $E\rightarrow 0$ to counteract the damping effects of the Boltzmann factor $E\exp(-E/kT)$, or that the treatment of the CO rotation is inadequate to model the intricate angular momentum couplings which occur in low-temperature relaxation processes. Ultimately, only a CS–CS calculation with a more accurate interaction potential will throw any light on the origin of the intriguing behavior observed in this system.

VI. SUMMARY

Good agreement is found between the present theoretical calculation and experiment and some past theoretical treatments, although agreement between these calculations and those of Schinke and co-workers is poor. For the CO–H_2 system, the lack of a direct coupling term in the potential was expected to lead to an underestimate of the influence of the near-resonant $\Delta J_{H_2}=4$ processes ($J=2\rightarrow 6$) on the relaxation rate constants. However, on comparison with previous studies and with experimental results the present potential does appear to give a qualitative, although not quantitative, understanding of the importance of this process on the vibrational deactivation of CO($v=1$) and of its influence on the differing rate constants for the pH_2 and oH_2 systems above 80 K. A reversal of the efficiency of the deactivating partners at temperatures below 80 K, the ortho-H_2 isomer being the more efficient collision partner, is expected on the basis of this calculation. This prediction has renewed experimental interest in this system with further experimental measurements of the rate constants for the deactivation of CO($v=1$) by para-H_2 planned to extend the existing data below 70 K. While clarifying the reasons for the ortho-/para-H_2 effect, this calculation has also resulted in an understanding of the

reasons why no such similar effect is observed for the CO–D_2 system at the temperatures at which experimental data currently exist.

An aim of the present calculations was to find an experimental explanation for the observation that the relaxation rate constants for the CO($v=1$)-nH_2 system increase for temperatures below 60 K. A significant upturn in the relaxation cross sections at impact energies below 60 cm^{-1} was found, but this was insufficient to produce an upturn in thermally averaged rate constants. The most significant deficiency of the present calculations is likely to be the use of the IOS approximation in the treatment of the CO rotation, rather than the use of an inaccurate interaction potential. The attractive well region of the interaction potential which was used in these calculations is much deeper than that for the CO–He and N_2–He systems,[27,28] and causes an upturn in cross sections at much higher collision energies. This qualitative behavior in the cross sections is unlikely to be altered by a more accurate interaction potential, indicating that a low-energy upturn in cross sections caused by the acceleration of the projectile molecule in the attractive part of the potential is not sufficient to produce a low-temperature upturn in relaxation rate constants. Additional enhancement of the cross sections due to rotational coupling of the light-mass projectile with the target molecule appears to play a crucial role in the relaxation process at low temperatures.

It is clear that there is a need for further calculations to be performed of the vibrational relaxation processes in these systems, using a potential which is more accurate, and which includes more detailed information about the dependence on the H_2 orientation angle. The determination of such an interaction potential surface is underway.[50] It is hoped to perform CS–CS calculations on this new potential surface although only for the CO–H_2 system since the larger basis set required for D_2 prohibits the application of a CS–CS treatment.

Further experimental work is also necessary, both to investigate whether an ortho–para effect exists for CO–H_2 at low temperatures, and to elucidate the mechanism by which upturns in the relaxation rate constants are generated. Experimental rate constant data for the vibrational relaxation of CO by pH_2 in the temperature range 35 K$<T<$80 K is sufficient to determine the relaxation rate constants for oH_2, because the data for the CO–nH_2 system are already available. Assuming that a low-temperature ortho–para effect does exist, a valuable insight into the mechanisms by which energy is transferred in diatom–diatom collisions at low temperatures, can be gained directly. The symmetry of the H_2 spin isomers restricts the relaxation pathways available to the two systems with the two pathways being mutually exclusive. If rotational coupling of the target and the projectile really is the most important factor in determining whether relaxation cross sections increase sufficiently at low impact energies to cause upturns in the relaxation rate constants at low temperatures, the further study of these systems will reveal whether it is odd- or even-parity rotational states which are the more efficient in causing the phenomenon. It is intended that such experiments be performed by members of this laboratory in the near future.

ACKNOWLEDGMENTS

We wish to thank the HPCI Grand Challenge Consortium, Glep (Chemical Reactions and Energy Exchange Processes), EPSRC Grant No. 41656, for enabling these calculations to be performed on the Edinburgh Cray T3D. We wish also to thank Dr. Ian Bush for his assistance in the use of the parallel version of MOLSCAT and Dr. Jeremy Hutson for his helpful advice at the start of this project. HMQ wishes to acknowledge the support of an EPSRC Advanced Fellowship.

[1] R. Schinke, H. Meyer, U. Buck, and G. H. F. Diercksen, J. Chem. Phys. **80**, 5518 (1984).
[2] Z. Bačić, R. Schinke, and G. H. F. Diercksen, J. Chem. Phys. **82**, 236 (1985).
[3] R. D. Sharma and C. W. Kern, J. Chem. Phys. **55**, 1171 (1971).
[4] C. I. Nelson and R. E. Roberts, Chem. Phys. **2**, 445 (1973).
[5] L. L. Poulsen and G. D. Billing, Chem. Phys. **73**, 313 (1982).
[6] G. Drolshagen and F. A. Gianturco, Mol. Phys. **48**, 673 (1983).
[7] G. Drolshagen and F. A. Gianturco, Mol. Phys. **54**, 185 (1984).
[8] D. J. Baker and D. R. Flower, J. Phys. B: At. Mol. Phys. **17**, 119 (1984).
[9] D. J. Baker and D. R. Flower, J. Phys. B: At. Mol. Phys. **17**, 3901 (1984).
[10] D. J. Baker and D. R. Flower, J. Phys. B: At. Mol. Phys. **17**, L829 (1984).
[11] Z. Bačić, R. Schinke, and G. H. F. Diercksen, J. Chem. Phys. **82**, 245 (1985).
[12] W. J. Hooker and R. C. Millikan, J. Chem. Phys. **38**, 214 (1963).
[13] R. C. Millikan and L. A. Osburg, J. Chem. Phys. **41**, 2196 (1964).
[14] D. J. Miller and R. C. Millikan, J. Chem. Phys. **53**, 3384 (1970).
[15] J. C. Stephenson and E. R. Mosburg, Jr., J. Chem. Phys. **60**, 3562 (1974).
[16] D. F. Starr, J. K. Hancock, and W. H. Green, J. Chem. Phys. **61**, 5421 (1974).
[17] A. J. Andrews and C. J. S. M. Simpson, Chem. Phys. Lett. **36**, 271 (1975).
[18] A. J. Andrews and C. J. S. M. Simpson, Chem. Phys. Lett. **41**, 565 (1976).
[19] C. J. S. M. Simpson, A. J. Andrews, and T. J. Price, Chem. Phys. Lett. **42**, 437 (1976).
[20] D. C. Allen and C. J. S. M. Simpson, Chem. Phys. **76**, 231 (1983).
[21] G. J. Wilson, M. L. Turnidge, A. S. Solodukhin, and C. J. S. M. Simpson, Chem. Phys. Lett. **207**, 521 (1993).
[22] M. L. Turnidge, G. J. Wilson, and C. J. S. M. Simpson, Chem. Phys. Lett. **227**, 45 (1994).
[23] J. Prissette, E. Kochanski, and D. R. Flower, Chem. Phys. **27**, 373 (1978).
[24] D. R. Flower, J. M. Launay, E. Kochanski, and J. Prissette, Chem. Phys. **37**, 355 (1979).
[25] L. L. Poulsen, Chem. Phys. **68**, 29 (1982).
[26] M. C. van Hemert, J. Chem. Phys. **78**, 2345 (1983).
[27] J. P. Reid, C. J. S. M. Simpson, and H. M. Quiney, Chem. Phys. Lett. **246**, 562 (1995).
[28] J. P. Reid, C. J. S. M. Simpson, and H. M. Quiney, Chem. Phys. Lett. **256**, 531 (1996).
[29] S. Green, J. Chem. Phys. **82**, 4548 (1985).
[30] A. Palma and S. Green, J. Chem. Phys. **85**, 1333 (1986).
[31] M. C. Salazar, A. De Castro, J. L. Paz, G. H. F. Diercksen, and A. J. Hernńdez, Int. J. Quantum Chem. **55**, 251 (1995).
[32] R. Moszynski, T. Korona, P. E. S. Wormer, and Ad van der Avoird, J. Chem. Phys. **103**, 321 (1995).
[33] C.-H. Hu and A. Thakkar, J. Chem. Phys. **104**, 2541 (1996).
[34] See, for example, G. C. Maitland, M. Rigby, E. B. Smith, and W. A. Wakeham, *Intermolecular Forces. Their Origin and Determination* (Clarendon, Oxford, 1981).
[35] G. A. Parker and R. T Pack, J. Chem. Phys. **64**, 2010 (1976).
[36] G. A. Parker and R. T Pack, J. Chem. Phys. **69**, 3268 (1978).

[37] W. Meyer, Chem. Phys. **17**, 27 (1976).
[38] L. D. Thomas, W. P. Kraemer, and G. H. F. Diercksen, Chem. Phys. **51**, 131 (1980).
[39] R. Schinke and G. H. F. Diercksen, J. Chem. Phys. **83**, 4516 (1985).
[40] See, for example, *Atom-Molecule Collision Theory*, edited by R. B. Bernstein (Plenum, New York, 1979), and references therein.
[41] J. M. Hutson and S. Green, MOLSCAT, Parallel computer code developed from version 12 (1993) of the serial code by I. J. Bush, distributed by Collaborative Computational Project No. 6 of the Science and Engineering Research Council, United Kingdom.
[42] D. E. Manolopoulos and M. H. Alexander, J. Chem. Phys. **86**, 2044 (1987).
[43] K. P. Huber and G. Herzberg, *Molecular Spectra and Molecular Structure IV. Constants of Diatomic Molecules* (Van Nostrand Reinhold, New York, 1979).
[44] D. C. Allen, T. Scragg, and C. J. S. M. Simpson, Chem. Phys. **51**, 279 (1980).
[45] J. P. Reid, C. J. S. M. Simpson, H. M. Quiney, and J. M. Hutson, J. Chem. Phys. **103**, 2528 (1995).
[46] P. Bréchignac, A. Picard-Bersellini, R. Charneau, and J. M. Launay, Chem. Phys. **53**, 165 (1980).
[47] J. Andres, U. Buck, H. Meyer, and J. M. Launay, J. Chem. Phys. **76**, 1417 (1982).
[48] G. D. Billing and L. L. Poulsen, Chem. Phys. **70**, 119 (1982).
[49] G. D. Billing and L. L. Poulsen, Chem. Phys. Lett. **99**, 368 (1983).
[50] R. Kobayashi (personal communication).